Self-Exchange Electron Transfer Kinetics and Reduction Potentials for Anthraquinone Disulfonate

Kevin M. Rosso,*,† Dayle M. A. Smith,‡ Zheming Wang,† Calvin C. Ainsworth,† and Jim K. Fredrickson†

Pacific Northwest National Laboratory, P.O. Box 999, K8-96, Richland, Washington 99352, and Department of Physics, Whitman College, 345 Boyer Avenue, Walla Walla, Washington 99362

Received: October 16, 2003; In Final Form: January 5, 2004

An electron transfer model for self-exchange reactions of 9,10-anthraquinone-2,6-disulfonate (AQDS) in aqueous solution has been formulated by using a combination of density functional theory (DFT) calculations and Marcus theory. One-electron self-exchange reactions are predicted to be fast (log $k \approx 6-9$ M^{-1} s^{-1}) but not diffusion limited. The internal component of the reorganization energy makes a large contribution to the total reorganization energy and cannot be neglected. Analysis and theoretical extensions of crystal structure data led to predicted precursor complex structures that, in the end, yielded theoretical electron transfer rates in good agreement with experimental ones. Electron transfer distances in solution are predicted to be in the 7−9 Å range. Calculated values of the electronic coupling matrix element indicate that the distinction between adiabatic and nonadiabatic electron transfer in this system likely occurs in this distance range as well. A set of reduction potentials was also produced by combining the density functional theory calculations with equilibrium expressions and the known acidity constants in the AQDS system.

Introduction

The redox behavior of quinones impacts many areas of biochemistry and environmental science. Transformation of quinones by gain or loss of electrons is an important natural process in biological energy conversion. Quinones also function as redox-active centers in natural organic matter, enabling donors and acceptors to utilize quinones as electron shuttle intermediates.[1−3] Recent evidence highlights the electron shuttling utility of quinones in the respiration of dissimilatory metal reducing bacteria.[4−6] Anthraquinone, the focus of this study, shows an electrochemically reversible apparent two-electron, two-proton reduction−oxidation reaction like most other quinones. The electron exchanges are thought to take place in successive one-electron steps leading to one-electron radical intermediates known as semiquinones.[7−9] Semiquinones have been shown to act as sensitizers to radiation damage to hypoxic cells and are therefore in use as antitumor drugs.[10,11] They also are being explored as photosensitizers in solar radiation-driven systems.[12,13]

Despite the importance of the electron transfer (ET) behavior of anthraquinones, little fundamental insight into individual steps in the overall ET process is currently available. Much of the early research was performed at a time when isolating one-ET reactions for detailed study was very difficult. More recently, rapid spectrophotometric techniques such as pulse radiolysis and Fourier transform electron spin resonance have helped to isolate semiquinones and one-electron reaction steps.[14−20] This has led to the quantification of half-cell potentials and intrinsic activation energy barriers for one-ET reactions. However, the knowledge of such quantities for each possible reactant pair in any given quinone system is usually incomplete. Theoretical models have the potential to help fill the knowledge gap.

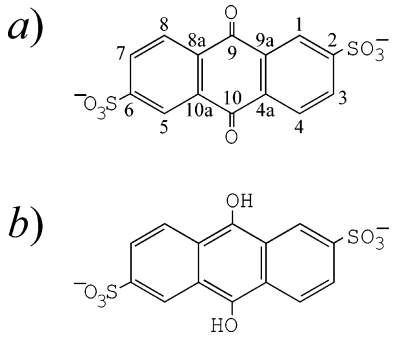

Figure 1. The Kekulé structures for (a) AQDS and (b) AH_2DS. The numbering scheme used throughout this study is given in part a.

In this study, we apply molecular modeling calculations and Marcus ET theory[21] to evaluate one-electron reduction potentials and self-exchange kinetics in the system 9,10-anthraquinone-2,6-disulfonate (AQDS). We chose this particular sulfonated derivative primarily because of its now routine application as a model electron shuttle in laboratory studies of natural aquatic and geomicrobiologic systems.[6,22−25] But we have also done so because there is reasonably good experimental data available for the reduction potentials and electron self-exchange kinetics for comparison with modeling results. In this study, we will examine some possible self-exchange ET reactions to understand the intrinsic ET behavior of the various species.

Background

The structures of the fully oxidized, unprotonated (AQDS) and fully reduced, protonated (AH_2DS) species and the IUPAC numbering system are shown in Figure 1. Relevant species and

* Address correspondence to this author. E-mail: kevin.rosso@pnl.gov. Phone: (509) 376-7762. Fax: (509) 376-3650.
† Pacific Northwest National Laboratory.
‡ Whitman College.

10.1021/jp037134u CCC: $27.50
Published on Web 03/26/2004

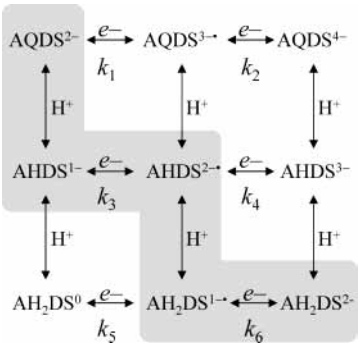

Figure 2. The nine-member square scheme for the AQDS system. A possible pathway between oxidized and reduced forms for mildly acidic conditions consisting of one-proton/one-electron steps is highlighted in gray.

the H^+ and e^- reactions between them can be understood from the nine-member square scheme[26] shown in Figure 2. This set of species will be referred to as the AQDS system. The protonation state of the quinone oxygen atoms is incremented across rows of the square scheme. The electronic state is incremented across columns from oxidized in the left column to semiquinone radicals in the middle column to reduced in the right column. The presence of the two sulfonate groups imparts a −2 net charge to the otherwise neutral deprotonated oxidized species in the upper left corner. Solvent properties such as pH and Eh dictate the equilibrium species distribution. The equilibrium speciation and reaction kinetics in this system have been well studied experimentally.[14−20,27−31]

The square scheme presents a way to conceptualize pathways from reduced to oxidized forms and vice versa in terms of simple successive electron and/or proton additions/subtractions. The particular route followed generally depends on the pH and pK_a values of the various intermediate species.[26] However, this simple view is far from reality in most cases. Disporportionation reactions between the radical anions can only be neglected under certain high pH conditions where the radical lifetimes are known to be long.[26,27] One also needs to be particularly concerned about the relative rates of proton and ET reactions and whether they are coupled.[15]

In many previous electrochemical kinetic studies, protonation reactions were assumed to be at equilibrium on the time scale of ET, and thus ET was regarded as rate-limiting.[26] Adopting this assumption, a possible oxidation reaction pathway starting from AH_2DS can be denoted as e^- H^+ e^- H^+ (Figure 2). Rates of such ET reactions in which the protonation states on reactants and products have been explicitly taken into account are poorly known. In this study we provide theoretical estimates for the six one-electron self-exchanges shown in Figure 2.

Methods

ET Model. Each one-electron self-exchange reaction is assumed to be an outer-sphere reaction involving the following steps: (1) diffusion of the reactants together to form the precursor complex, (2) ET within the complex to form the successor complex, and (3) dissociation of the successor complex. For example, for the self-exchange ET pair $AQDS^{2-}$/$AQDS^{3-\bullet}$, these steps can be written as

$$AQDS^{2-} + AQDS^{3-\bullet} \xleftrightarrow{k_d/k_{-d}} AQDS^{2-}\cdots AQDS^{3-\bullet} \quad (1)$$

$$AQDS^{2-}\cdots AQDS^{3-\bullet} \xleftrightarrow{k_{et}/k_{-et}} AQDS^{3-\bullet}\cdots AQDS^{2-} \quad (2)$$

$$AQDS^{3-\bullet}\cdots AQDS^{2-} \rightarrow AQDS^{3-\bullet} + AQDS^{2-} \quad (3)$$

Applying the steady-state approximation to the concentrations of the precursor and successor complexes, the overall observable ET rate (k_{obs}) is given by[21]

$$\frac{1}{k_{obs}} = \frac{1}{K}\frac{1}{k_{et}} + \frac{1}{k_d} \quad (4)$$

where K is the equilibrium constant for the formation of the precursor complex, k_{et} is the rate of ET, and k_d is the rate of diffusion-controlled precursor complex formation. Because the intrinsic ET rates in this system are close to the diffusion limit, the effect of k_d on the overall rate must be accounted for. Also, because of the presence of the anionic sulfonate groups in the current system, most of the reactions considered here are between two negatively charged reactants. Therefore, implicit in the model descriptions that follow is the need to account for the Coulombic repulsions between the reactants. We take k_d as[28]

$$k_d = \frac{2RT}{3\eta}\left(\frac{\delta}{e^{\delta}-1}\right)\left(\frac{{d_{ij}}^2}{r_i r_j}\right) \quad (5)$$

where R is the gas constant, T is the temperature, η is the solvent viscosity (taken as 8.94×10^{-7} kPa·s), $\delta = w_{ij}/RT$, where w_{ij} is the work to bring the reactants i and j together to form the precursor complex at the separation distance d_{ij}, and r_i and r_j are the reactant radii. Equation 5 assumes spherical reactants. Because the reactants in our system are better described as ellipsoidal, effective "mean" radii were computed for the ellipsoids, as described in a later section below, and were used in eq 5.

The equilibrium constant for precursor complex formation K is based on the reaction zone model and is given by[32]

$$K = \frac{4\pi N_A {d_{ij}}^2 \partial d}{1000}\exp(-w_{ij}/RT) \quad (6)$$

where N_A is Avogadro's number and ∂d is the effective reaction zone thickness. The latter corresponds to the range in distances over which the ET rate is appreciable.[33] Here we use $\partial d = 0.8$ Å as is usually done.[33−35]

The work term w_{ij} was computed by using Coulomb's law, which gives the electric potential energy for bringing two point charges together to a separation distance d_{ij} as

$$w_{ij} = \frac{1}{4\pi\epsilon_0}\frac{z_i z_j e^2 N_A}{\epsilon_s d_{ij}} \quad (7)$$

where $1/4\pi\epsilon_0 = 8.99 \times 10^9$ N·m^2·C^{-2}, z_i and z_j are the charges of the reactants, e is the elementary charge, and ϵ_s is the static dielectric constant of water (taken as 78.39). This estimate of w_{ij} ignores other possible interactions between the reactants, presuming they are outweighed by the Coulombic interactions because most of the reactions considered occur between two charged reactants. Its application also implies zero ionic strength.

The rate of the ET step was calculated with Marcus theory in the nonadiabatic limit, which gives[34]

$$k_{et} = \frac{2\pi}{\hbar}V_{AB}^2\frac{e^{-(\Delta G^{o\prime}+\lambda)^2/4\lambda RT}}{\sqrt{4\pi\lambda RT}} \quad (8)$$

where $\hbar$ is Planck's constant, V_{AB} is the matrix element

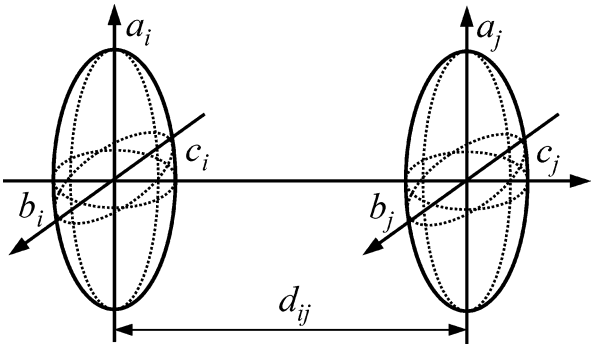

Figure 3. Relative cavity positions and orientations and definitions of semiaxes in the continuum external reorganization energy model of German and Kuznetsov.[42]

describing the coupling of the electronic state of the reactants to that of the products, $\Delta G^{\circ\prime}$ is the free energy of reaction corrected for the work to bring the reactants together and the products together in the encounter complex, and λ is the energy to reorganize the nuclear coordinates of the reactants and surrounding solvent molecules into the configuration compatible with ET. The nonadiabatic treatment was selected based on calculations of the transmission coefficient κ, which always gave $\kappa < 1$. Transmission coefficients were calculated as described earlier[36] by using the Landau−Zener method[33,37−39] as well as Sutin's method, which is based on the Landau−Zener method.[32,40] For the latter, the aromatic carbon−carbon stretching frequency (i.e., for −C═C− linkages 1457 cm^{-1})[41] was used as the frequency of nuclear motion. Landau−Zener and Sutin's methods yielded essentially identical transmission coefficients.

The reorganization energy was assumed to be separable into two main contributions. The internal part (λ_I) is due to the energy required to reorganize bonds in the precursor complex to a configuration compatible with ET. The external part (λ_E) is due to energy required to adjust the polarization of the solvent molecules surrounding the complex to a configuration compatible with ET. λ_I was calculated by using ab initio methods, described in a later section. Because of the ellipsoidal shape of the AQDS species, the external reorganization energy was calculated by using the continuum equation of German and Kuznetsov[42] for conducting ellipsoids. The external reorganization energy is given by

$$\lambda_E = e^2\left(\frac{1}{\epsilon_{opt}} - \frac{1}{\epsilon_s}\right)\left(\frac{1}{2}\sum_{n=i}^{j}\frac{F(\phi_n,\alpha_n)}{\sqrt{a_n^2 - c_n^2}} - \frac{1}{d_{ij}}\right) \quad (9)$$

where ϵ_{opt} is the optical dielectric constant of water, taken as the square of the index of refraction for water, and $F(\phi_n,\alpha_n)$ is the elliptic integral of the first kind where the parameters

$$\phi_n = \sin^{-1}\left(\frac{\sqrt{a_n^2 - c_n^2}}{a_n}\right) \quad (10)$$

and

$$\alpha_n = \sin^{-1}\sqrt{\frac{a_n^2 - b_n^2}{a_n^2 - c_n^2}} \quad (11)$$

and a_n, b_n, and c_n are the semiaxes of ellipsoid n (Figure 3). The semiaxes must be $a_n > b_n > c_n$. Note that the application of this model assumes that λ_E for the computed precursor complexes is well approximated by symmetrically oriented ellipsoids (Figure 3).[42] By comparison with the Marcus continuum equation for spherical cavities,[21] eq 9 allows for the definition of a "mean" spherical radius $\bar{r}$ for each ellipsoid as

$$\bar{r} \equiv \frac{\sqrt{a_n^2 - c_n^2}}{F(\phi_n,\alpha_n)} \quad (12)$$

that is roughly approximated by but not equivalent to the average of a_n, b_n, and c_n. The semiaxes for all AQDS species were estimated from the dimensions of the van der Waals surface along orthogonal directions for the ab initio optimized $AQDS^{2-}$ structure. The calculated $\bar{r}$ was used as r_i and r_j in eq 5 to estimate k_d.

Finally, we note that the rate expression used to predict an overall rate constant for comparison with k_{obs} (eq 4) depends on the relative rates of internal reorganization, external reorganization, and electron hopping at the nuclear configuration appropriate for electron transfer.[33] For example, if the vibrational dynamics responsible for relaxing the reorganized successor complex are slow relative to the electron hopping rate then the relaxation time must be known to properly describe the overall ET rate. In the model as described above, it has been tacitly assumed that the rate of ET is not controlled by an internal or external relaxation process for this system.[33,43−47]

Precursor Complex Structure. Because of V_{AB}, the ET rate is highly dependent on the distance and relative orientation of the reactant molecules in the precursor complex.[33,34,48−51] For ET in solution at room temperature, there is likely a thermally populated distribution of precursor complex structures at any given time. Without a priori knowledge of the most probable precursor complex structures, V_{AB} would need to be computed for a series of randomly generated structures and suitably averaged by using some weighting scheme.[52] Here we circumvent this laborious procedure by attempting to determine those precursor complex structures that are likely to be dominant and therefore outweigh the others in such an average. Computing V_{AB} explicitly for those is then assumed to come close to the average. It was assumed that the most probable approach distances and relative orientations for the self-exchange pairs considered would mimic the arrangement of AH_2DS molecules in its corresponding solid-phase salt structure. For the molecules in this study, the nearest crystal structure analogue available is for sodium 9,10-dihydroanthraquinone-1,5-disulfonate trihydrate (AH_2DS salt hydrate).[53] Gamage and co-workers also determined that sulfonate substitution in the 1-position versus 2-position has only limited impact on the atomic positions and lattice parameters.

Here we utilized molecular mechanics methods to predict the changes in the crystal structure upon altering the sulfonate substitution pattern from 1,5 to 2,6 using the Gamage et al. structure[53] as the starting configuration. The structure optimization was performed with use of periodic boundary conditions as implemented in the Cerius2 package (Accelrys, Inc.). Hydrogen positions were not determined in Gamage et al.[53] because they used X-ray methods. Hydrogen atoms were added to the starting structure manually to complete the description of the structure and also to neutralize the unit cell charge. Approximating hydrogen positions was unambiguous except for those belonging to hydrate waters in the sodium planes, where water dipoles were chosen to be aligned parallel to the *ac* plane. Connectivity was evaluated by using covalent radii and a

bonding tolerance factor of 1.15 so that a bond was found if the distance between two atoms was less than 115% of the sum of their covalent radii. The model was parametrized using the universal force field,[54] which has been shown to be accurate for organic molecules.[55] Fractional atomic charges were calculated for the Gamage et al. structure[53] using the charge equilibration method.[56] The unit cell edges and atomic positions were then optimized (unit cell angles fixed) without symmetry constraints. Two constraints were applied during the optimization. The anthraquinone "backbones" of individual AH_2DS molecules in the unit cell were constrained to move as internally fixed rigid bodies. The two sodium layers in the unit cell were also each constrained to move as rigid bodies. Starting from the resulting optimized structure, sulfonate groups were manually moved from 1,5 positions to 2,6 positions in orientations consistent with rotation of the groups into the new sites. The same optimization procedure was then repeated, yielding the relaxed structure of 9,10-dihydroanthraquinone-2,6-disulfonate trihydrate.

Two AQDS pairs were excised from the optimized structure based on the two shortest center-to-center distances. These two "supermolecular" pairs were used as precursor complex templates for the ab initio calculations described below. Ab initio optimized structures of the various AQDS species were fit as rigid bodies onto the positions in the precursor complex templates with use of a least-squares routine.

Structure Optimizations. Gas-phase optimized structures for each of the nine members of the AQDS system (Figure 2) were computed with the open-shell B3LYP hybrid DFT functional.[57] B3LYP uses a weighted sum of Hartree−Fock (exact) exchange, Slater's local spin density approximation for exchange,[58] Becke's gradient corrected expression for exchange,[59] the VWN local correlation functional,[60] and the LYP correlation functional.[61] B3LYP has been shown to perform very well for quinone and polycyclic aromatic systems.[62−70] We used the Pople-type triple-ζ plus polarization 6-311G(d,p) basis set for all atoms.[71] All B3LYP calculations were performed with Gaussian98.[72]

Internal Reorganization Energy. The internal reorganization energy for each self-exchange reaction was computed with Nelsen's 4-point method,[73] with the necessary energies computed using the gas-phase ab initio methods described above. This method has been successfully applied to ET systems where the reactants are structurally distinct units (e.g., in an outer-sphere precursor complex in solution) or are connected by a long molecular bridge.[36,74−80] The 4-point method is not applicable to reactants that are in a strongly coupled unit, which usually occurs between units connected by direct bonding or by a short bridge.[81] Thus, use of the 4-point method here assumes the reactants are independent of each other.

Electronic Coupling Matrix Element. Self-exchange ET reactions can be described in terms of two symmetric diabatic potential energy surfaces with respect to a nuclear configurational coordinate q.[21] Electron transfer is instantaneous with respect to motion of the nuclei.[82,83] Thermally promoted ET occurs at the crossing-point configuration (q_C) between the ground-state configurations of the reactants (q_A) and of the products (q_B). q_C corresponds to the intersection of the (parabolic) potential energy surfaces for the reactants and products, which in our case of self-exchange ET are symmetrically equivalent surfaces. Electronic interaction between the reactant and product states at q_C, described by the electronic coupling matrix element V_{AB}, leads to splitting of the surfaces in the crossing-point region. V_{AB} is half of the energy splitting between the upper and lower adiabatic surfaces at q_C, which gives

$$V_{AB} = \frac{|H_{AB} - S_{AB}(H_{AA} + H_{BB})/2|}{1 - {S_{AB}}^2} \tag{13}$$

where $H_{AB} = \langle\psi_A|H|\psi_B\rangle$ and $S_{AB} = \langle\psi_A|\psi_B\rangle$, where A and B designate reactants and products, respectively, and H is the total electronic Hamiltonian. The state ψ_A is the wave function for the reactants at q_C, and ψ_B is the wave function for the products at q_C. The calculation of V_{AB} was performed for the two precursor complexes, using the ab initio approach by Farazdel and co-workers[84] as implemented in NWChem.[85] The ET module in NWChem uses the method of corresponding orbital transformation to bi-orthogonalize the overlap between the spin−orbitals of the ET states A and B, thereby simplifying the evaluation of the Hamiltonian between them by using Slater's rules.[86] We performed the V_{AB} calculations at the spin-unrestricted Hartree−Fock (UHF) level using the 3-21+G basis set.[87−90]

To determine the crossing point configuration q_C, we used the linearized reaction coordinate approximation. When the ET products and reactants energy curves are parabolic, a good approximation of the reaction coordinate is given by[84]

$$q(\xi) = \xi q_A + (1 - \xi) q_B \tag{14}$$

By using $1 \geq \xi \geq 0$, q can smoothly change from q_A ($\xi = 1$) to q_B ($\xi = 0$) going through q_C ($\xi = 1/2$).

Reduction Potentials. For future application of the current calculations to cross-reactions, we extended our calculations to evaluate some of the important standard reduction potentials for aqueous solution reactions in this system. We adopted a common thermodynamic cycle strategy to relate standard reduction potentials in aqueous solution to electron affinities in the gas-phase and solvation free energies (ΔG_{solv}) (Figure 4).[63,66,91−94] The standard reduction potential for the upper left-to-right reaction in Figure 4 is approximated using the alternative path by summing computed solvation free energies for the separate reactants and the reduction free energy (an electron affinity term) for the gas-phase donor/acceptor couple. Gas-phase ab initio optimizations very similar to those used here have been shown to give electron affinities to within 0.05 eV on average for a series of substituted benzoquinones.[63,64] Because it has been shown that the reduction free energy is closely approximated by the reduction enthalpy for quinone systems,[95,96] here we use ΔH_{red} as the energy for the reduction step. We computed the enthalpy of each of the AQDS species by performing a frequency calculation in Gaussian98[72] on the structures optimized in the gas phase using B3LYP as described above. The frequency calculations in Gaussian98 also produce an estimate of the zero-point energy correction and are followed by statistical thermodynamic analysis of the thermal correction

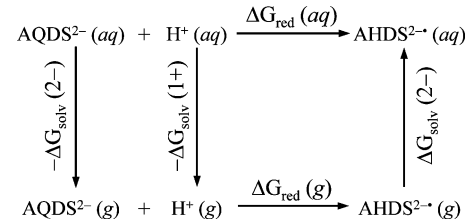

Figure 4. An example thermodynamic cycle scheme for computing the reduction potential with ab initio methods. See the text for discussion.

TABLE 1: A Comparison between Calculated and Experimentally Determined Structural Parameters[a]

	9,10-anthraquinone-2,6-disulfonate	9,10-anthraquinone			9,10-anthraquinone-1,5-disulfonate
	UB3LYP/6-311G(d,p) (this study)	gas-phase electron diffraction[102]	UB3LYP/6-31G(d)[62]	single-crystal X-ray diffraction[103]	single-crystal X-ray diffraction[53]
C1−C2	1.392	1.400	1.392	1.382	1.393
C2−C3	1.398	1.400	1.400	1.392	1.391
C8a−C9	1.491	1.499	1.492	1.492	1.498
C9−O	1.224	1.220	1.226	1.225	1.217
C1−H	1.082	1.087	1.085	0.972	-
O−C9−C8a	121.1	121.3	121.3	120.8	118.1
C1−C2−C3	119.7	119.8	120.1	120.0	120.9

[a] See Figure 1 for the atom numbering scheme. Bond lengths are in Ångstroms and angles are in degrees.

for translational, rotational, and vibrational motions for the hypothetical 1 atm ideal gas standard state at 298.15 K. While this choice of standard state pressure is not applicable to solution conditions,[97] the error that is introduced cancels itself in the evaluation of the reduction potentials.

The value for the solvation free energy for a proton in water was taken from Zhan and Dixon.[98] For the various AQDS species, we computed the solvation free energy in water using two different forms of continuum approximation. The first-order continuum approximation used was the Born model

$$\Delta G_{\text{solv}} = -\frac{z^2}{2r}\left(1 - \frac{1}{\epsilon_s}\right) \qquad (15)$$

where z is the charge of the molecule and r is the radius of its cavity in solution. Here we take $\bar{r}$ as defined in eq 12 as r in eq 15.

The second method used is the polarized continuum model (PCM) of Tomasi and co-workers in conjunction with the ab initio calculations.[99,100] The PCM is a more detailed approach that accounts explicitly for the molecular shape of the solute cavity, and also accounts for certain nonelectrostatic terms such as the cavitation energy and solute−solvent dispersion interaction. Various PCM definitions of the solute cavity have been put forward, such as using the union of overlapping atom-centered spheres, using a static electron density isosurface or one that is determined self-consistently. After determining that such differences make negligible differences in the apparent accuracy of the solvation energy for $AQDS^{2-}$, we chose to use the less-expensive method of overlapping spheres to define the solute cavities. Sphere radii were chosen according to the united atom topological model.[101] Hydrogen atoms are enclosed in the sphere of the atom to which they are bonded. Like the Born model, the PCM defines area outside the solute cavity as a continuum of dielectric constant ϵ_s, which may be polarized in response to dipoles in the solute.

Results and Discussion

Structures. Optimized structures of the AQDS species at the UB3LYP/6-311G(d,p) level show excellent correspondence to the nearest available experimental structures. To the best of our knowledge, no experimental gas-phase or crystal structure determinations have been made specifically for the 2,6-sulfonated derivative of 9,10-anthraquinone. However, the structure of 9,10-anthraquinone is well studied by both electron diffraction methods on gas-phase molecules[102] and X-ray diffraction methods on various related crystal structures.[103,104] Also, the structures of 9,10-anthraquinone-1,5-disulfonate[53] and anthraquinone-1,8-disulfone potassium salt dihydrate[105] have been determined. A comparison of bond lengths and angles between those computed here for $AQDS^{2-}$ and closely related structures reported elsewhere is given in Table 1. It should be emphasized that the performance of the UB3LYP/6-311G(d,p) method for describing bond lengths and energies in this system is not in question, because of the high accuracy that was demonstrated previously on closely related systems.[62−64,66,68−70,94,106,107] Average absolute deviations between the 9,10-anthraquinone structure calculated with UB3LYP/6-31G(d) and the experimental gas-phase structure are 0.003 Å for bonds and 0.4° for bond angles.[62] A similar level of accuracy is found here.

Analysis of Mulliken spin density population of the three semiquinone radicals (Figure 2) shows a relatively uniform distribution of spin density among the carbon atoms ($\rho_\alpha - \rho_\beta \sim \pm 0.03-0.08$), suggesting that an added electron is indeed inserted into a delocalized π-system, as expected. When a hydrogen atom is present on a quinone oxygen, spin density of similar magnitude as found on each of the carbon atoms is found on that oxygen as well. However, the spin density on unprotonated quinone oxygen atoms is larger than that of any of the other atoms by an order of magnitude ($\rho_\alpha - \rho_\beta \sim \pm 0.2$), suggesting that the added electron is more strongly localized when unprotonated quinone oxygen atoms are present. This is consistent with previous modeling studies.[62] Sulfur atoms and their associated oxygen atoms of the sulfonate groups, as well as hydrogen atoms, exhibit negligible spin density.

Changes in the structures of the oxidized species upon reduction to semiquinone radicals and further on to fully reduced species results predominantly in bond length changes, which are tabulated in Table 2. In general, the bond length changes are small, no greater than ±0.04 Å (±2.3%) on average, and systematic, showing a alternating pattern of bond length increases and decreases as one follows the sequence of carbon−carbon bonds around the aromatic system (Figure 5a). They also usually progress in the same manner from the first one-electron reduction to the second; a bond length increase after one-electron addition is generally followed by an additional increase after the second electron addition, and likewise for bond length decreases. The small bond length changes are consistent with a change of bond order that is widely distributed over many bonds in the π-system.

The alternation of bond length increases/decreases upon progressive changes in the number of electrons can be understood from the distribution of the lowest unoccupied molecular orbital (LUMO) of one of the oxidized species, which is the accepting orbital for additional electrons. Carbon and quinone oxygen atomic orbitals of 2p character combine to form this part of the π-system. An isosurface plot of the LUMO calculated for $AQDS^{2-}$ and a schematic version are shown in Figure 5, parts b and c, respectively. Discontinuous areas correspond to the locations of nodal planes in the LUMO and regions of

TABLE 2: Bond Lengths (Å) and Percent Bond Length Changes (in parentheses) upon One-Electron Addition Calculated for the AQDS System, Using Gas-Phase Optimizations at the UB3LYP/6-311G(d,p) Level[a]

	AQDS			AHDS			AH_2DS		
bond	−2, 1	−3, 2	−4, 1	−1, 1	−2, 2	−3, 1	0, 1	−1, 2	−2, 1
C1−C2	1.392	1.380 (−0.9)	1.380 (0.0)	1.403	1.386 (−1.2)	1.380 (−0.4)	1.379	1.385 (0.4)	1.365 (−1.4)
C2−C3	1.398	1.416 (1.3)	1.432 (1.1)	1.400	1.407 (0.5)	1.419 (0.9)	1.406	1.408 (0.1)	1.423 (1.1)
C3−C4	1.388	1.377 (−0.8)	1.375 (−0.1)	1.380	1.377 (−0.2)	1.371 (−0.4)	1.380	1.376 (−0.3)	1.366 (−0.7)
C4−C4a	1.399	1.415 (1.1)	1.423 (0.6)	1.413	1.421 (0.6)	1.433 (0.8)	1.412	1.418 (0.4)	1.432 (1.0)
C4a−C10	1.491	1.467 (−1.6)	1.452 (−1.0)	1.429	1.424 (−0.3)	1.403 (−1.5)	1.424	1.417 (−0.5)	1.403 (−1.0)
C10−C10a	1.492	1.466 (−1.7)	1.452 (−1.0)	1.432	1.424 (−0.6)	1.404 (−1.4)	1.427	1.426 (−0.1)	1.405 (−1.5)
C10a−C5	1.399	1.419 (1.4)	1.429 (0.7)	1.406	1.419 (0.9)	1.436 (1.2)	1.409	1.408 (−0.1)	1.430 (1.6)
C5−C6	1.392	1.379 (−0.9)	1.380 (0.1)	1.390	1.379 (−0.8)	1.373 (−0.4)	1.379	1.385 (0.4)	1.367 (−1.3)
C6−C7	1.398	1.416 (1.3)	1.432 (1.1)	1.396	1.409 (0.9)	1.419 (0.7)	1.406	1.409 (0.2)	1.425 (1.1)
C7−C8	1.388	1.377 (−0.8)	1.375 (−0.1)	1.397	1.382 (−1.1)	1.379 (−0.2)	1.380	1.375 (−0.4)	1.366 (−0.7)
C8−C8a	1.399	1.415 (1.1)	1.423 (0.6)	1.485	1.404 (−5.5)	1.411 (0.5)	1.412	1.418 (0.4)	1.429 (0.8)
C8a−C9	1.491	1.468 (−1.5)	1.452 (−1.1)	1.499	1.476 (−1.5)	1.467 (−0.6)	1.424	1.417 (−0.5)	1.404 (−0.9)
C9−C9a	1.492	1.467 (−1.7)	1.452 (−1.0)	1.383	1.479 (6.9)	1.466 (−0.9)	1.427	1.426 (−0.1)	1.405 (−1.5)
C9a−C1	1.399	1.419 (1.4)	1.429 (0.7)	1.403	1.404 (0.1)	1.417 (0.9)	1.409	1.408 (−0.1)	1.430 (1.6)
C8a−C10a	1.409	1.426 (1.2)	1.456 (2.1)	1.420	1.422 (0.1)	1.441 (1.3)	1.429	1.432 (0.2)	1.440 (0.6)
C9a−C4a	1.409	1.426 (1.2)	1.456 (2.1)	1.424	1.427 (0.2)	1.442 (1.1)	1.429	1.433 (0.3)	1.444 (0.8)
C9−O	1.224	1.258 (2.8)	1.288 (2.4)	1.217	1.237 (1.6)	1.257 (1.6)	1.331*	1.340* (0.7)	1.376* (2.7)
C10−O	1.224	1.258 (2.8)	1.288 (2.4)	1.321*	1.363* (3.2)	1.413* (3.7)	1.331*	1.341* (0.8)	1.382* (3.1)
C2−S	1.831	1.824 (−0.4)	1.818 (−0.3)	1.824	1.826 (0.1)	1.818 (−0.4)	1.815	1.826 (0.6)	1.822 (−0.2)
C6−S	1.831	1.824 (−0.4)	1.817 (−0.4)	1.833	1.829 (−0.2)	1.825 (−0.2)	1.815	1.826 (0.6)	1.824 (−0.1)

[a] Species are labeled as in Figure 2 and the molecular charge and spin multiplicity are given immediately beneath the labels. See Figure 1 for the atom numbering scheme. Quinone oxygen atoms possessing a proton are designated with an asterisk.

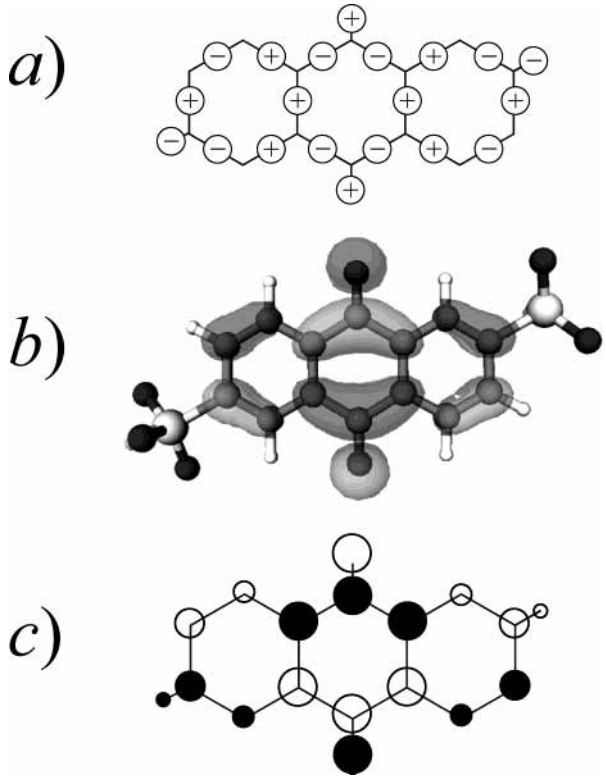

Figure 5. (a) Depiction of the pattern of bond length distortions that occur in the AQDS system upon one- and two-electron reduction. A plus (minus) sign indicates a bond length increase (decrease). (b) The calculated isosurface of the lowest unoccupied molecular orbital (LUMO) for $AQDS^{2-}$. (c) An alternative depiction of the LUMO qualitatively but more clearly showing its amplitude (circle size), sign (circle color), and the location of nodal planes for $AQDS^{2-}$. Bond length increases indicated in part a occur between atoms where the LUMO character is antibonding, as indicated in part c by a change in sign.

antibonding interaction between adjacent atoms, while continuous areas correspond to bonding interactions (Figure 5b). Reduction of $AQDS^{2-}$ involves filling this orbital, destablizing (lengthening) bonds where the LUMO character is antibonding and stabilizing (shortening) bonds where the LUMO character is bonding. This leads to distortion of the structure in the pattern shown in Figure 5a (see also Table 2). This distortion pattern is not the same as that found for the well-studied compound anthracene.[74,108,109] Calculated energy differences associated with one-electron reduction steps, such as electron affinities and reorganization energies, are discussed below.

TABLE 3: Solvation Free Energies Computed with Two Different Continuum Models and Calculated Reduction Energies, Using Energies for Gas-Phase Structures Optimized at the UB3LYP/6-311G(d,p) Level

$\Delta\Delta G_{solv}$ (*e*V)			$\Delta\Delta G_{solv}$ (*e*V) PCM	ΔH_{red} (*e*V)
$AQDS^{2-}$	→	$AQDS^{3-\bullet}$	-6.6	2.97
-6.3	Born	-14.2		
-6.2	PCM	-12.8		
$AQDS^{3-\bullet}$	→	$AQDS^{4-}$	-10.1	7.20
-14.2	Born	-25.3		
-12.8	PCM	-22.9		
$AHDS^{1-}$	→	$AHDS^{2-\bullet}$	-3.5	-1.48
-1.6	Born	-6.3		
-3.1	PCM	-6.6		
$AHDS^{2-\bullet}$	→	$AHDS^{3-}$	-6.5	2.71
-6.3	Born	-14.2		
-6.6	PCM	-13.1		
AH_2DS^{0}	→	$AH_2DS^{1-\bullet}$	-1.0	-4.98
0.0	Born	-1.6		
-2.4	PCM	-3.4		
$AH_2DS^{1-\bullet}$	→	AH_2DS^{2-}	-3.3	-1.58
-1.6	Born	-6.3		
-3.4	PCM	-6.7		

Reduction Potentials. In this section, we consider the calculated energy differences associated with one- and two-electron reduction steps shown in Figure 2. The objective is to predict the standard reduction potentials by using the scheme shown in Figure 4. First we examine separately the calculated electron affinities and solvation free energies.

The energy of the reduction step, ΔH_{red}, calculated for structures optimized at the UB3LYP/6-311G(d,p) level for the six one-electron steps (Figure 2) are given in Table 3. Although, to the best of our knowledge, no experimental electron affinities

for our specific system are available for comparison, previous modeling work suggests the electron affinities calculated in this way should be accurate to within approximately 0.05 eV.[63,64] As expected, the electron affinities become more negative as protons are added to an isoelectronic series (any vertical sequence in Figure 2) because of the progressively more positive net charge offset. For an isostructural series (any horizontal sequence in Figure 2), the electron affinity becomes more positive for the addition of a second electron primarily for the same reason. The electron affinities of like charged species are similar but slightly more positive for the less protonated species (e.g., 2.97 eV for $AQDS^{2-}$ and 2.71 eV for $AHDS^{2-\bullet}$, −1.48 eV for $AHDS^{2-}$ and −1.58 eV for $AH_2DS^{1-\bullet}$).

Calculated solvation free energies using two different polarizable continuum models are also given in Table 3. Because the Born model assumes a more simplistic solute cavity shape, it is assumed to give a poorer ΔG_{solv} estimate. The PCM is assumed to give a better estimate due to its more accurate treatment of the cavity shape and inclusion of nonelectrostatic terms such as the solute−solvent dispersion interaction energy. While the computed values for ΔG_{solv} are of similar magnitude for the two methods, there is generally a disparity between them that is large relative to the level of accuracy that is reportedly obtainable for polarized continuum models.[93] The best agreement obtained is for the species having a 2− charge (standard deviation = 0.3 eV).

Calculated reduction potentials with comparisons to experimental ones are given in Table 4. To the best of our knowledge, only formal reduction potentials are available for this system. Formal reduction potentials depend on pH, ionic strength, and the type of acid/base involved.[110] The best agreement between calculated and experimental reduction potentials was obtained for the charge balanced reduction equations involving protons:

$$AQDS^{2-} + 2e^- + 2H^+ \rightarrow AH_2DS^{2-} \quad (16)$$

$$AQDS^{2-} + e^- + H^+ \rightarrow AHDS^{2-\bullet} \quad (17)$$

$$AHDS^{2-\bullet} + e^- + H^+ \rightarrow AH_2DS^{2-} \quad (18)$$

Calculation of the ΔG_{solv} component for the above reduction potentials involves PCM calculations that are for like-charged (2−) reactant and product AQDS species. This was deemed the best strategy as it affords the possibility that some of the absolute solvation energy errors inherent to a PCM calculation may cancel in the evaluation of $\Delta\Delta G_{solv}$. This also leads to a smaller contribution from $\Delta\Delta G_{solv}$ to the reduction potential than from the electron affinity contribution, which is a more accurate calculation. In contrast to these reduction potentials, one-electron reduction potentials calculated in the same way that do not involve protons gave unsatisfactory agreement with experiment, likely due to inaccuracies introduced into $\Delta\Delta G_{solv}$ from the PCM model. It is well-known that specific interactions between functional groups and solvent molecules, especially for radical species, in the first solvation sphere sometimes make crucial contributions to the solvation free energy that are missed by treating first-shell water as part of the solvent continuum.[62,91,93,111] Thus, several of the remaining reduction potentials in Table 4 were computed indirectly, using equilibrium expressions[110] with reduction potentials calculated for the charge-balanced reactions above in combination with the acidity constants for AH_2DS^{2-} ($pK_{r1} = 8.1$) and $AHDS^{3-}$ ($pK_{r2} = 10.5$)[7] and $AHDS^{2-\bullet}$ ($pK_r = 3.2$)[28,30] as explained in the table footnotes. This approach yielded an internally consistent reduction potential set that compares reasonably well with experimental formal reduction potentials where known (Table 4). Finally, we remind the reader that the reduction potentials produced here are meant for future application of the Marcus cross-relation to reduction reactions involving the AQDS system; they do not have a role in the self-exchange kinetics discussed below.

TABLE 4: A Comparison of Calculated Standard Two- and One-Electron Reduction Potentials with Nearest Equivalent Experimental Reduction Potentials (all potentials are with respect to the standard hydrogen electrode (SHE) at room temperature)

reduction reaction	calcd $E°$ (V, SHE)	expt[a] (V, SHE)
two-electron:		
$AQDS^{2-} + 2e^- + 2H^+ \rightarrow AH_2DS^{2-}$	0.253	$E_0 = 0.228$,[b] $E_0 = 0.263$[c]
$AQDS^{2-} + 2e^- \rightarrow AQDS^{4-}$	−0.298[d]	−0.323[e]
one-electron:		
$AQDS^{2-} + e^- + H^+ \rightarrow AHDS^{2-\bullet}$	−0.055	−0.066[f]
$AHDS^{2\bullet-} + e^- + H^+ \rightarrow AH_2DS^{2-}$	0.561	0.522[g]
$AQDS^{2-} + e^- \rightarrow AQDS^{3-\bullet}$	−0.244[h]	$E_7^1 = -0.255$[i]
$AQDS^{3-\bullet} + e^- \rightarrow AQDS^{4-}$	−0.351[j]	−0.391[k]
		$E_7^2 = -0.146$,[l] $E_?^2 = -0.222$[m]
$AHDS^- + e^- \rightarrow AHDS^{2-\bullet}$	−0.012[n]	
$AHDS^{2-\bullet} + e^- \rightarrow AHDS^{3-}$	−0.085[n]	$E_{0.3}^2 = -0.048$[o]
$AH_2DS^0 + e^- \rightarrow AH_2DS^{-\bullet}$	0.341[n]	
$AH_2DS^{-\bullet} + e^- \rightarrow AH_2DS^{2-}$	−0.002[n]	

[a] To the best of our knowledge, no true standard reduction potentials ($E°$) have been reported. Where E_0 is specified the listed potential is a formal, rather than standard, potential and is pH dependent. E_0 approximates the standard reduction potential at pH 0 (H^+ at unit activity) and only under certain conditions depending on the ionic strength and acid used.[110] Where E_y^x is specified, the listed potential is a formal first ($x = 1$) or second ($x = 2$) one-electron reduction potential at pH y. [b] This is a formal reduction potential (pH 0) from Clark.[7] [c] This is a formal reduction potential (pH 0) estimated from Figure 7 of Albery et al.[27] [d] Computed by applying eq 27 of Wardman[110] to the calculated 0.253 V value, using $pK'_{r1} = 8.1$ and $pK'_{r2} = 10.5$.[7] [e] Computed as in footnote *d*, except using Clark's[7] experimental $E_0 = 0.228$ V. [f] Estimated by applying eq 45 of Wardman[110] to the $E_7^1 = -0.255$ value of Pal,[16] using $pK'_r = 3.2$ for $AHDS^{2-\bullet}$.[28,30] [g] Because of the strong pH dependence of E[2,16] this value was estimated by using eq 6 of Wardman,[110] using Clark's[7] experimental $E_0 = 0.228$ V and the "experimental" value estimated in footnote *f*. [h] Computed as in footnote *f*, except with the calculated −0.055 V value. [i] From Pal.[16] This value is the same at pH 11. [j] Computed by applying eq 54c of Wardman[110] to the calculated 0.561 V value, using $pK'_{r1} = 8.1$, $pK'_{r2} = 10.5$,[7] and $pK'_o = 3.2$ for $AHDS^{2-\bullet}$.[28,30] [k] Computed as in footnote *j*, except using the value estimated in footnote *g*. [l] From Pal.[16] This value is sensitive to pH and changes to −0.244 V at pH 11. [m] Gamage et al.[30] See also Table 1 of Grampp et al.[28] [n] Approximated by using calculated electron affinities and predicted values for $\Delta\Delta G_{solv}$. $\Delta\Delta G_{solv}$ was predicted from the reduction potentials and corresponding calculated electron affinities in footnotes *h* and *j*, and also from the changes in $\Delta\Delta G_{solv}$ for like-charged species having different protonation states predicted by the PCM method. [o] From Table 1 of Grampp et al.[28] The value changes to −0.151 at pH 2.

Precursor Complex. To predict rates of self-exchange ET between the various AQDS species, V_{AB} must be accurately known. As explained above, we chose to compute V_{AB} only for likely precursor complex structures, rather than using an averaged V_{AB} for a random sampling of all possible structures (see Methods section). We assume that reasonable models for precursor complex structures can be found in the crystal structure of AH_2DS. This further assumes that as the AH_2DS molecules condense into the crystalline state, forces of interaction between them are sufficiently minimized. The molecular mechanics calculations used to optimize the 9,10-anthraquinone-2,6-

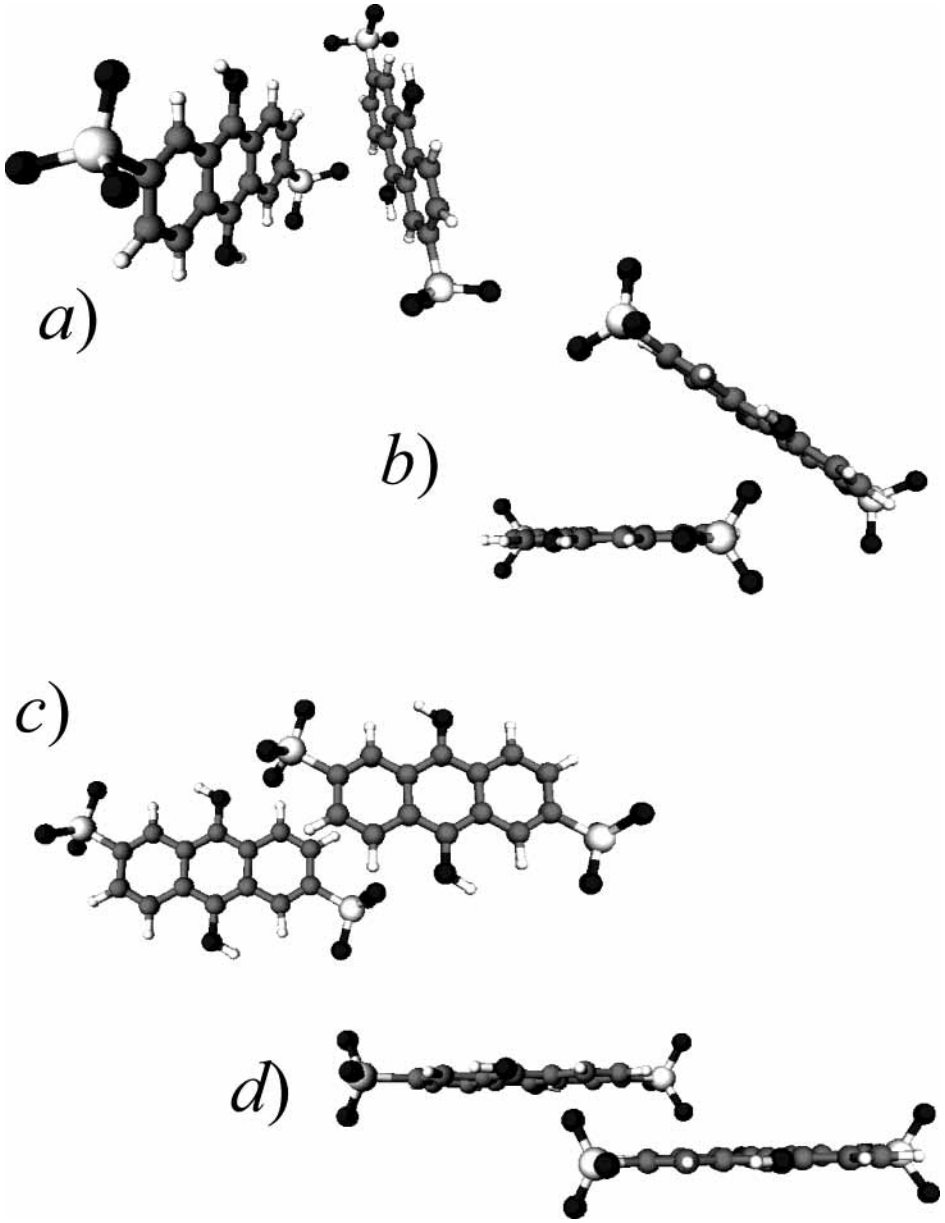

Figure 6. Two different views of ball-and-stick models showing the two predicted precursor complexes. The SR configuration is shown in parts a and b. The LP configuration is shown in parts c and d.

disulfonate trihydrate starting from the experimental 1,5-disulfonated structure determined by Gamage et al.[53] performed well. Optimization of the 1,5 structure gave lattice parameters and atomic coordinates that are close to the reported structure and converged to the same space group (*Pnma*). This structure is provided in Table 1S in the Supporting Information. The decrease in the *b*-axis length arises from a slight rotation of the AQDS molecules that leads to a slightly more compact structure. Optimization of the subsequently derived 2,6 structure resulted primarily in additional internal rotation in response to the displacement of the sulfonate groups from 1,5 to more distal 2,6 positions. Other than a reduction of the symmetry to $P2_1/m$, the predicted 2,6 structure (Table 2S in the Supporting Information) possesses most of the characteristics of the 1,5 structure.

Two pairs of AH_2DS molecules having the two shortest center-to-center distances were excised for use as templates for precursor complex structures. The pair yielding the shortest center-to-center distance (7.09 Å) can be characterized as possessing centers staggered along the long axes and noncoplanar AH_2DS planes (Figure 6a,b). These AH_2DS molecules are ~37° out of coplanarity. This configuration will be hereafter referred to as the short, rotated (SR) configuration. The second pair yielding the next shortest center-to-center distance (9.00 Å) also possesses staggered centers but has parallel AH_2DS configurations (Figure 6c,d). This configuration will be hereafter referred to as the long, parallel (LP) configuration. As expected, in both configurations the negatively charged sulfonate groups are far from those of the opposing partner molecule and generally are offset so as to coincide with the central part of the opposing partner molecule. The staggering of molecular centers that is a characteristic of both of these precursor complexes is very similar to precursor complex structures found for closely related systems and has been rationalized on the basis of minimization of the electrostatic energy.[47] These two supermolecular pairs of AH_2DS molecules were used as model precursor complex templates for explicit evaluation of V_{AB} as described next.

TABLE 5: Calculated Values for the Internal Reorganizaton Energy for the Six One-Electron Self-Exchange Reactions Diagrammed in Figure 2[a]

self-exchange reaction	λ_I (eV)
$AQDS^{2-} + AQDS^{3-\bullet} \rightarrow AQDS^{3-\bullet} + AQDS^{2-}$	0.455
$AQDS^{3-\bullet} + AQDS^{4-} \rightarrow AQDS^{4-} + AQDS^{3-\bullet}$	0.404
$AHDS^{-} + AHDS^{2-\bullet} \rightarrow AHDS^{2-\bullet} + AHDS^{-}$	0.303
$AHDS^{2-\bullet} + AHDS^{3-} \rightarrow AHDS^{3-} + AHDS^{2-\bullet}$	0.412
$AH_2DS^{0} + AH_2DS^{-\bullet} \rightarrow AH_2DS^{-\bullet} + AH_2DS^{0}$	0.423
$AH_2DS^{-\bullet} + AH_2DS^{2-} \rightarrow AH_2DS^{2-} + AH_2DS^{-\bullet}$	0.394

[a] Values were calculated by using the electronic energies from the UB3LYP/6-311G(d,p) optimizations and Nelsen's 4-point method.[73]

Electronic Coupling Matrix Element. The V_{AB} term was directly computed for the following self-exchange reaction

$$AH_2DS^{1-\bullet} + AH_2DS^{2-} \rightarrow AH_2DS^{2-} + AH_2DS^{1-\bullet} \quad (19)$$

(which is the reaction corresponding to k_6 in Figure 2) for each of the two precursor complex models. Structures of $AH_2DS^{1-\bullet}$ and AH_2DS^{2-} optimized at the UB3LYP/6-311G(d,p) level were fit as rigid bodies onto each of the two precursor complex templates. For each template, this was done twice: once for the initial state geometry before ET (reactants state) and once for the final state geometry after ET (products state). The crossing-point geometries ($\zeta = 0.5$) were computed by using a linearized reaction coordinate model,[84] and these q_C geometries for both the SR and LP configurations are given in Table 3S of the Supporting Information. The wave functions for the reactant state at q_C, the product state at q_C, and evaluation of V_{AB} were computed at the UHF/3-21+G level.

The resulting V_{AB} for the SR configuration is 0.056 eV and for the LP configuration it is 0.032 eV. The lower V_{AB} for the LP configuration is consistent with the larger center-to-center distance of separation by 1.9 Å relative to the SR configuration. These values turn out to be significantly higher than the prediction by Jortner,[44] whose theoretical work on parallel stacked naphthalene and anthracene molecules gave

$$V_{AB}\,(\text{eV}) = 12.398 \exp(-\alpha d_{ij}) \quad (20)$$

where $\alpha = 1.0$ Å^{-1} is the decay constant with d_{ij} the separation as defined earlier. This expression yields $V_{AB} = 0.010$ (SR) and 0.002 eV (LP), which differ markedly from our directly calculated values above. We attribute the differences to differences in the relative positions and orientations for our precursor complexes compared to the idealized configurations in Jortner's modeling study. More surprising is the observation that our configurations with the molecular centers staggered lead to larger V_{AB} values than Jortner's prediction for perfectly aligned centers where generally greater orbital overlap would be anticipated. This may indicate a contribution to V_{AB} from the quinone oxygen groups present in the current system.

Reorganization Energies. Internal reorganization energies computed with Nelsen's 4-point method[73] for the six self-exchange reactions shown in Figure 2 are given in Table 5. Nelsen's method was previously shown to give relatively consistent results independent of basis set.[78] As was done in our calculations, the inclusion of electron correlation was shown to be important for benzene, naphthalene, and anthracene.[74] Calculated values for λ_I vary somewhat about the average value of 0.4 eV but there is no apparent simple correlation between λ_I and the protonation states of the reactant pair. In general, the λ_I values are larger than might be anticipated given the small bond length changes incurred upon loss/gain of an electron (Table 2). Values calculated here are in reasonable agreement with λ_I estimated for $AQDS^{2-}/AQDS^{3-\bullet}$ and $AHDS^{1-}/AHDS^{2-\bullet}$ self-exchange reactions with use of a Marcus analysis of experimental rate data (0.323 eV).[28] They are much higher than anticipated for self-exchange reactions of anthracene.[74,112,113] In fact, as shown below, λ_I is large enough to have a significant impact on the ET rate.

In kinetic models of many ET reactions involving aromatic systems in polar solvents, λ_I is often assumed to be negligible relative the external reorganization energy (λ_E).[9,114] This is not the case for the current system. As described in the Methods section, we calculated a "mean" radius for an ellipsoidal solute cavity containing each of the AQDS species in this study to be 4.5 Å, according to eqs 9−12.[42] Taking d_{ij} for the SR configuration (7.09 Å), $\lambda_E = 0.667$ eV. For the LP configuration ($d_{ij} = 9.00$ Å) $\lambda_E = 0.905$ eV, higher than for the SR configuration solely because of the increased ET distance. Thus, the total reorganization energies computed for the two configurations are in the range of 1.0−1.4 eV, of which the internal part of the reorganization energy comprises ~25−41%. These values for λ_E do not change significantly by including the subtle changes in the dimensions of the solute cavity due to changing the protonation state of the quinone. Therefore λ_E values for the two configurations are chosen to be independent of the particular AQDS species considered in an ET rate calculation.

Self-Exchange Rates. Evaluation of the transmission coefficient κ at the crossing-point configuration led to $\kappa < 1$ in all cases. Therefore k_{et} was evaluated using the nonadiabatic treatment. Rate constant terms for the six self-exchange reactions are listed in Table 6 for the SR configuration and Table 7 for the LP configuration. These were computed for aqueous solution conditions at room temperature in the limit of zero ionic strength. The larger λ_E for the LP configuration leads to a higher activation free energy ΔG^*, causing a general decrease in k_{et}. The equilibrium constant for precursor complex formation K is lower for self-exchange reactions in the SR configuration because of the closer distance of approach. The diffusion-limited rate k_d is faster than $k_{et} \times K$ in all cases for both configurations, which means the ET reactions are not diffusion limited. The overall observable rate of ET varies between 3.4 and 8.6 log units for the SR configuration (Table 6) and between 3.2 and

TABLE 6: Calculated Self-Exchange Rate Parameters for the Short, Rotated (SR) Configuration Treated Nonadiabatically[a]

self-exchange reaction	λ (eV)	κ	ΔG^* (eV)	logk_{et} (s^{-1})	log$K$ (M^{-1})	logk_d ($M^{-1}s^{-1}$)	logk_{obs} ($M^{-1}s^{-1}$)
$AQDS^{2-} + AQDS^{3-\bullet} \rightarrow AQDS^{3-\bullet} + AQDS^{2-}$	1.122	0.61	0.280	8.96	−3.14	7.83	5.81
$AQDS^{3-\bullet} + AQDS^{4-} \rightarrow AQDS^{4-} + AQDS^{3-\bullet}$	1.071	0.61	0.268	9.19	−5.77	5.50	3.41
$AHDS^{-} + AHDS^{2-\bullet} \rightarrow AHDS^{2-\bullet} + AHDS^{-}$	0.970	0.63	0.243	9.63	−1.39	9.16	8.19
$AHDS^{2-\bullet} + AHDS^{3-} \rightarrow AHDS^{3-} + AHDS^{2-\bullet}$	1.079	0.61	0.270	9.15	−3.14	7.83	6.00
$AH_2DS^{0} + AH_2DS^{-\bullet} \rightarrow AH_2DS^{-\bullet} + AH_2DS^{0}$	1.090	0.61	0.273	9.10	−0.52	9.87	8.56
$AH_2DS^{-\bullet} + AH_2DS^{2-} \rightarrow AH_2DS^{2-} + AH_2DS^{-\bullet}$	1.061	0.61	0.265	9.23	−1.39	9.16	7.82

[a] The conditions are for room temperature aqueous solution in the limit of infinite dilution (zero ionic strength). The ET distance is 7.09 Å and $V_{AB} = 0.056$ eV.

TABLE 7: Calculated Self-Exchange Rate Parameters for the Long, Parallel (LP) Configuration Treated Nonadiabatically[a]

self-exchange reaction	λ (eV)	κ	ΔG^* (eV)	logk_{et} (s^{-1})	log$K$ (M^{-1})	logk_d ($M^{-1}\,s^{-1}$)	logk_{obs} ($M^{-1}\,s^{-1}$)
$AQDS^{2-} + AQDS^{3-\bullet} \rightarrow AQDS^{3-\bullet} + AQDS^{2-}$	1.360	0.27	0.340	7.42	−2.38	8.49	5.04
$AQDS^{3-\bullet} + AQDS^{4-} \rightarrow AQDS^{4-} + AQDS^{3-\bullet}$	1.309	0.27	0.327	7.65	−4.45	6.72	3.20
$AHDS^{-} + AHDS^{2-\bullet} \rightarrow AHDS^{2-\bullet} + AHDS^{-}$	1.208	0.28	0.302	8.09	−1.00	9.49	7.09
$AHDS^{2-\bullet} + AHDS^{3-} \rightarrow AHDS^{3-} + AHDS^{2-\bullet}$	1.317	0.27	0.329	7.61	−2.38	8.49	5.23
$AH_2DS^{0} + AH_2DS^{-\bullet} \rightarrow AH_2DS^{-\bullet} + AH_2DS^{0}$	1.328	0.27	0.332	7.56	−0.31	9.87	7.25
$AH_2DS^{-\bullet} + AH_2DS^{2-} \rightarrow AH_2DS^{2-} + AH_2DS^{-\bullet}$	1.299	0.27	0.325	7.69	−1.00	9.49	6.69

[a] The conditions are for room temperature aqueous solution in the limit of infinite dilution (zero ionic strength). The ET distance is 9.00 Å and $V_{AB} = 0.032$ eV.

7.2 log units for the LP configuration (Table 7). Variability in k_{obs} from one self-exchange reaction to another for either of the SR and LP configurations turns out to arise primarily from K and not from k_{et}. A one-to-one comparison of SR and LP configuration rates for any one self-exchange reaction shows that the 1.9 Å longer distance of separation in the LP configuration leads to a decrease in log k_{obs} by an average of 1.6 ± 0.3 log units. Thus, assuming that the precursor complexes selected in this study are accurate representations of probable precursor complexes in solution, ET reactants achieving the SR precursor complex configuration are predicted to dominate the flux of the self-exchange reaction.

Calculated values of k_{obs} reported in Tables 6 and 7 compare reasonably well with available measured rates for this AQDS system and closely related systems. Rates for specific self-exchange reactions including the protonation state on both sides of the reaction are not commonly available. However, Grampp et al.[28] modeled photoinduced ET reactions of 9,10-anthraquinone-2,6-disulfonate based on experimental rate data. In that study, a log k_{obs} of 6.38 was found for the reaction $AQDS^{2-} + AQDS^{3-\bullet} \rightarrow AQDS^{3-\bullet} + AQDS^{2-}$, which compares reasonably well with our value of log $k_{obs} = 5.81$ for the SR configuration. Also, Grampp et al.[28] found a log k_{obs} of 6.93 for the reaction $AHDS^{1-} + AHDS^{2-\bullet} \rightarrow AHDS^{2-\bullet} + AHDS^{1-}$, which is shifted in the right direction but compares less well with our value of 8.19 for the SR configuration. Many measured rates for self-exchange reactions for similar systems of unspecified speciation conditions have been reported. There is variability in these rates in the range of log $k_{obs} = 6-9$,[9,18,20] consistent in general with the range of values found in this study for the SR configuration (Table 6). Varying protonation states as well as differences in the location of the sulfonate groups have been shown to have a strong effect on the ET rate.[14,29] The findings in this study confirm the former.

Conclusions

An ET model for self-exchange reactions in the 9,10-anthraquinone-2,6-disulfonate system has been formulated. A combination of DFT electronic structure calculations and Marcus ET theory was successfully applied to compute the physical quantities underlying the rate behavior. The electronic structure calculations were also used to varying degrees of success to estimate standard reduction potentials for the half-cell reactions. Inconsistencies in polarizable continuum models led to uncertainties in the solvation free energies that were generally unsatisfactory. However, a reasonable set of reduction potentials was produced by using a subset of the PCM results in combination with equilibrium expressions and the known acidity constants in the AQDS system.

One-electron self-exchange reactions are predicted to be fast but not diffusion limited. The internal component of the reorganization energy makes a large contribution to the total reorganization energy and cannot be neglected. Analysis and theoretical extensions of crystal structure data led to two predicted precursor complex structures that, in the end, yielded theoretical ET rates in good agreement with experimental ones. ET distances are therefore predicted to be in the 7−9 Å range. Values of the electronic coupling evaluated for the two precursor complex structures indicate that the distinction between adiabatic and nonadiabatic ET in this system likely occurs in this distance range as well. It is hoped that these findings will aid in the advancement of more detailed models of ET cross-reactions involving AQDS and its related species.

Acknowledgment. This work was made possible by a grant from the U.S. Department of Energy, Office of Biological and Environmental Research, Natural and Accelerated Bioremediation Research (NABIR Program). This work was supported in part by the Office of Advanced Scientific Computing Research, Office of Science, U.S. Department of Energy. The calculations were performed in part at the Molecular Science Computing Facility (MSCF) in the William R. Wiley Environmental Molecular Sciences Laboratory at the Pacific Northwest National Laboratory. The MSCF is funded by the Office of Biological and Environmental Research in the U.S. Department of Energy. The Pacific Northwest National Laboratory is operated by Battelle for the U.S. Department of Energy under Contract DE-AC06-76RLO 1830.

Supporting Information Available: Tables providing the calculated sodium 9,10-hydroanthraquinone-1,5-disulfonate trihydrate crystal structure, the sodium 9,10-hydroanthraquinone-2,6-disulfonate trihydrate crystal structure, and the two predicted crossing-point structures for the SR and LP encounter complexes. This material is available free of charge via the Internet at http://pubs.acs.org.

References and Notes

(1) Nurmi, J. T.; Tratnyek, P. G. *Environ. Sci. Technol.* **2002**, *36*, 617−624.

(2) Glaus, M. A.; Heijman, C. G.; Schwarzenbach, R. P.; Zeyer, J. *Appl. Environ. Microbiol.* **1992**, *58*, 1945−1951.

(3) Schwarzenbach, R. P.; Stierli, R.; Lanz, K.; Zeyer, J. *Environ. Sci. Technol.* **1990**, *24*, 1566−1574.

(4) Fredrickson, J. K.; Zachara, J. M.; Kennedy, D. W.; Dong, H. L.; Onstott, T. C.; Hinman, N. W.; Li, S. M. *Geochim. Cosmochim. Acta* **1998**, *62*, 3239−3257.

(5) Newman, D. K.; Kolter, R. *Nature* **2000**, *405*, 94−97.

(6) Zachara, J. M.; Fredrickson, J. K.; Li, S. M.; Kennedy, D. W.; Smith, S. C.; Gassman, P. L. *Am. Mineral.* **1998**, *83*, 1426−1443.

(7) Clark, W. M. *Oxidation−reduction potentials of organic systems*; The Williams & Wilkins Co.: Baltimore, MD, 1960.

(8) Chambers, J. Q. Electrochemistry of quinones. In *The Chemistry of Quinonoid Compounds*; Patai, S., Rappoport, Z., Eds.; Wiley: New York, 1988; Vol. 2, pp 719−757.

(9) Meisel, D.; Fessenden, R. W. *J. Am. Chem. Soc.* **1976**, *98*, 7505−7510.

(10) Gianni, L.; Corden, B. J.; Myers, C. E. The biochemical basis of anthracycline toxicity and antitumor activity. In *Reviews in Biochemical*

Toxicology; Hodgson, E., Bend, J., Philpot, R. M., Eds.; Elsevier: New York, 1983; pp 1−82.

(11) Neta, P. Radiation chemistry of quinonoid compounds. In *The Chemistry of Quinonoid Compounds*; Patai, S., Rappoport, Z., Eds.; Wiley: New York, 1988; Vol. 2, pp 879−898.

(12) Keita, B.; Nadjo, L. *J. Electroanal. Chem.* **1984**, *163*, 171−188.

(13) Keita, B.; Nadjo, L. *J. Electroanal. Chem.* **1983**, *151*, 283−288.

(14) Sauberlich, J.; Brede, O.; Beckert, D. *J. Phys. Chem. A* **1997**, *101*, 5659−5665.

(15) Loeff, I.; Rabani, J.; Treinin, A.; Linschitz, H. *J. Am. Chem. Soc.* **1993**, *115*, 8933−8942.

(16) Pal, H.; Palit, D. K.; Mukherjee, T.; Mittal, J. P. *Radiat. Phys. Chem.* **1991**, *37*, 227−235.

(17) Rath, M. C.; Pal, H.; Mukherjee, T. *Radiat. Phys. Chem.* **1996**, *47*, 221−227.

(18) Beckert, D.; Fessenden, R. W. *J. Phys. Chem.* **1996**, *100*, 1622−1629.

(19) Pal, H.; Palit, D. K.; Mukherjee, T.; Mittal, J. P. *J. Chem. Soc., Faraday Trans.* **1992**, *88*, 681−687.

(20) Das, S.; Bhattacharya, A.; Mandal, P. C.; Rath, M. C.; Mukherjee, T. *Radiat. Phys. Chem.* **2002**, *65*, 93−100.

(21) Marcus, R. A. *J. Chem. Phys.* **1956**, *24*, 966−978.

(22) Shyu, J. B. H.; Lies, D. P.; Newman, D. K. *J. Bacteriol.* **2002**, *184*, 1806−1810.

(23) Coates, J. D.; Cole, K. A.; Chakraborty, R.; O'Connor, S. M.; Achenbach, L. A. *Appl. Environ. Microbiol.* **2002**, *68*, 2445−2452.

(24) Ona-Nguema, G.; Abdelmoula, M.; Jorand, F.; Benali, O.; Gehin, A.; Block, J. C.; Genin, J. M. R. *Hyperfine Interact.* **2002**, *139*, 231−237.

(25) Kukkadapu, R. K.; Zachara, J. M.; Smith, S. C.; Fredrickson, J. K.; Liu, C. X. *Geochim. Cosmochim. Acta* **2001**, *65*, 2913−2924.

(26) Laviron, E. *J. Electroanal. Chem.* **1983**, *146*, 15−36.

(27) Albery, W. J.; Archer, M. D.; Field, N. J.; Turner, A. D. *Faraday Discuss. Chem. Soc.* **1973**, *56*, 28−40.

(28) Grampp, G.; Galan, M.; Sacher, M. *Ber. Bunsen-Ges. Phys. Chem. Chem. Phys.* **1995**, *99*, 111−117.

(29) Forster, R. J.; O'Kelly, J. P. *J. Electroanal. Chem.* **2001**, *498*, 127−135.

(30) Gamage, R.; McQuillan, A. J.; Peake, B. M. *J. Chem. Soc., Faraday Trans.* **1991**, *87*, 3653−3660.

(31) Wipf, D. O.; Wehmeyer, K. R.; Wightman, R. M. *J. Org. Chem.* **1986**, *51*, 4760−4764.

(32) Sutin, N. Theory of electron transfer reactions. In *Electron transfer and electochemical reactions; Photochemical and other energized reactions*; Zuckermann, J. J., Ed.; VCH: Weinheim, Germany, 1986; Vol. 15, pp 16−47.

(33) Newton, M. D.; Sutin, N. *Annu. Rev. Phys. Chem.* **1984**, *35*, 437−480.

(34) Marcus, R. A.; Sutin, N. *Biochim. Biophys. Acta* **1985**, *811*, 265−322.

(35) Gratzel, M. *Heterogeneous photochemical electron transfer*; CRC Press: Boca Raton, FL, 1989.

(36) Rosso, K. M.; Smith, D. M. A.; Dupuis, M. *J. Phys. Chem. A* Submitted for publication.

(37) Landau, L. *Phys. Z. Sowjetunion* **1932**, *1*, 89.

(38) Landau, L. *Phys. Z. Sowjetunion* **1932**, *2*, 46.

(39) Zener, C. *Proc. R. Soc.* **1932**, *A137*, 696.

(40) Brunschwig, B. S.; Logan, J.; Newton, M. D.; Sutin, N. *J. Am. Chem. Soc.* **1980**, *102*, 5798−5809.

(41) Klimkans, A.; Larsson, S. *Int. J. Quantum Chem.* **2000**, *77*, 211−220.

(42) German, E. D.; Kuznetsov, A. M. *Electrochim. Acta* **1981**, *26*, 1595−1608.

(43) Onuchic, J. N. *J. Chem. Phys.* **1987**, *86*, 3925−3943.

(44) Jortner, J.; Bixon, M. *J. Chem. Phys.* **1988**, *88*, 167−170.

(45) Sumi, H.; Marcus, R. A.; Arthur Amos Noyes Lab. Chem. Phys., C.I.T.P.C.A.U.S.A. *J. Chem. Phys.* **1986**, *84*, 4272−4276.

(46) Grampp, G.; Rauhut, G. *J. Phys. Chem.* **1995**, *99*, 1815−1817.

(47) Grampp, G.; Jaenicke, W. *Ber. Bunsen-Ges. Phys. Chem. Chem. Phys.* **1991**, *95*, 904−927.

(48) Tsue, H.; Nakashima, S.; Goto, Y.; Tatemitsu, H.; Misumi, S.; Abraham, R. J.; Asahi, T.; Tanaka, Y.; Okada, T.; Mataga, N.; Sakata, Y. *Bull. Chem. Soc. Jpn.* **1994**, *67*, 3067−3075.

(49) Sakata, Y.; Nakashima, S.; Goto, Y.; Tatemitsu, H.; Misumi, S.; Asahi, T.; Hagihara, M.; Nishikawa, S.; Okada, T.; Mataga, N. *J. Am. Chem. Soc.* **1989**, *111*, 8979−8981.

(50) Cave, R. J.; Klippenstein, S. J.; Marcus, R. A.; Arthur Amos Noyes Lab. Chem. Phys., C.I.T.P.C.A.U.S.A. *J. Chem. Phys.* **1986**, *84*, 3089−3098.

(51) Cave, R. J.; Siders, P.; Marcus, R. A.; Arthur Amos Noyes Lab. Chem. Phys., C.I.T.P.C.A.U.S.A. *J. Phys. Chem.* **1986**, *90*, 1436−1444.

(52) Gao, Y. Q.; Georgievskii, Y.; Marcus, R. A. *J. Chem. Phys.* **2000**, *112*, 3358−3369.

(53) Gamage, R. S. K. A.; Peake, B. M.; Simpson, J. *Aust. J. Chem.* **1993**, *46*, 1595−1604.

(54) Rappe, A. K.; Casewit, C. J.; Colwell, K. S.; Goddard, W. A.; Skiff, W. M. *J. Am. Chem. Soc.* **1992**, *114*, 10024−10035.

(55) Casewit, C. J.; Colwell, K. S.; Rappe, A. K. *J. Am. Chem. Soc.* **1992**, *114*, 10035−10046.

(56) Rappe, A. K.; Goddard, W. A. *J. Phys. Chem.* **1991**, *95*, 3358−3363.

(57) Becke, A. D. *J. Chem. Phys.* **1993**, *98*, 1372−1377.

(58) Slater, J. C. *Quantum Theory of Molecules and Solids*; McGraw-Hill: New York, 1974; Vol. 4.

(59) Becke, A. D. *Phys. Rev. A* **1988**, *38*, 3098−3100.

(60) Vosko, S. H.; Wilk, L.; Nusair, M. *Can. J. Phys.* **1980**, *58*, 1200−1211.

(61) Lee, C. T.; Yang, W. T.; Parr, R. G. *Phys. Rev. B* **1988**, *37*, 785−789.

(62) Grafton, A. K.; Wheeler, R. A. *J. Phys. Chem. A* **1997**, *101*, 7154−7166.

(63) Raymond, K. S.; Grafton, A. K.; Wheeler, R. A. *J. Phys. Chem. B* **1997**, *101*, 623−631.

(64) Boesch, S. E.; Grafton, A. K.; Wheeler, R. A. *J. Phys. Chem.* **1996**, *100*, 10083−10087.

(65) Reynolds, C. A. *Int. J. Quantum Chem.* **1995**, *56*, 677−687.

(66) Wheeler, R. A. *J. Am. Chem. Soc.* **1994**, *116*, 11048−11051.

(67) Jeziorek, D.; Ossowski, T.; Liwo, A.; Dyl, D.; Nowacka, M.; Woznicki, W. *J. Chem. Soc., Perkin Trans. 2* **1997**, 229−236.

(68) Matsuura, A.; Nishinaga, T.; Komatsu, K. *J. Am. Chem. Soc.* **2000**, *122*, 10007−10016.

(69) Dessent, C. E. H. *Chem. Phys. Lett.* **2000**, *330*, 180−187.

(70) Torii, H.; Ueno, Y.; Sakamoto, A.; Tasumi, M. *J. Phys. Chem. A* **1999**, *103*, 5557−5566.

(71) Hehre, W. J.; Radom, L.; Schleyer, P. v. R.; Pople, J. A. *Ab Initio Molecular Orbital Theory*; Wiley: New York, 1986.

(72) Frisch, M. J.; Trucks, G. W.; Schlegel, H. B.; Scuseria, G. E.; Robb, M. A.; Cheeseman, J. R.; Zakrzewski, V. G.; Montgomery, J. A., Jr.; Stratmann, R. E.; Burant, J. C.; Dapprich, S.; Millam, J. M.; Daniels, A. D.; Kudin, K. N.; Strain, M. C.; Farkas, O.; Tomasi, J.; Barone, V.; Cossi, M.; Cammi, R.; Mennucci, B.; Pomelli, C.; Adamo, C.; Clifford, S.; Ochterski, J.; Petersson, G. A.; Ayala, P. Y.; Cui, Q.; Morokuma, K.; Malick, D. K.; Rabuck, A. D.; Raghavachari, K.; Foresman, J. B.; Cioslowski, J.; Ortiz, J. V.; Stefanov, B. B.; Liu, G.; Liashenko, A.; Piskorz, P.; Komaromi, I.; Gomperts, R.; Martin, R. L.; Fox, D. J.; Keith, T.; Al-Laham, M. A.; Peng, C. Y.; Nanayakkara, A.; Gonzalez, C.; Challacombe, M.; Gill, P. M. W.; Johnson, B. G.; Chen, W.; Wong, M. W.; Andres, J. L.; Head-Gordon, M.; Replogle, E. S.; Pople, J. A. *Gaussian 98*, revision A.4; Gaussian, Inc.: Pittsburgh, PA, 1998.

(73) Nelsen, S. F.; Blackstock, S. C.; Kim, Y. *J. Am. Chem. Soc.* **1987**, *109*, 677−682.

(74) Klimkans, A.; Larsson, S. *Chem. Phys.* **1994**, *189*, 25−31.

(75) Rosso, K. M.; Rustad, J. R. *J. Phys. Chem. A* **2000**, *104*, 6718−6725.

(76) Eggleston, C. M.; Stack, A. G.; Rosso, K. M.; Higgins, S. R.; Bice, A. M.; Boese, S. W.; Pribyl, R. D.; Nichols, J. J. *Geochim. Cosmochim. Acta* **2003**, *67*, 985−1000.

(77) Zhang, X. D.; Wang, Y. N.; Guo, J. X.; Zhang, Q. Y. *J. Photochem. Photobiol. A* **1999**, *121*, 1−6.

(78) Kelterer, A. M.; Landgraf, S.; Grampp, G. *Spectrochim. Acta, Part A* **2001**, *57*, 1959−1969.

(79) Stack, A. G.; Rosso, K. M.; Smith, D. M. A.; Eggleston, C. *J. Colloid Interface Sci.* Submitted for publication.

(80) Rosso, K. M.; Morgan, J. J. *Geochim. Cosmochim. Acta* **2002**, *66*, 4223−4233.

(81) Rosso, K. M.; Smith, D. M. A.; Dupuis, M. *J. Chem. Phys.* **2003**, *118*, 6455−6466.

(82) Franck, J. *Trans. Faraday Soc.* **1925**, *21*, 536.

(83) Condon, E. U. *Phys. Rev.* **1928**, *32*, 858.

(84) Farazdel, A.; Dupuis, M.; Clementi, E.; Aviram, A. *J. Am. Chem. Soc.* **1990**, *112*, 4206−4214.

(85) Apra, E.; Bylaska, E. J.; de Jong, W.; Hackler, M. T.; Hirata, S.; Pollack, L.; Smith, D. M. A.; Straatsma, T. P.; Windus, T. L.; Harrison, R. J.; Nieplocha, J.; Tipparaju, V.; Kumar, M.; Brown, E.; Cisneros, G.; Dupuis, M.; Fann, G. I.; Fruchtl, H.; Garza, J.; Hirao, K.; Kendall, R.; Nichols, J. A.; Tsemekhman, K.; Valiev, M.; Wolinski, K.; Anchell, J.; Bernholdt, D.; Borowski, P.; Clark, T.; Clerc, D.; Dachsel, H.; Deegan, M.; Dyall, K.; Elwood, D.; Glendening, E.; Gutowski, M.; Hess, A.; Jaffe, J.; Johnson, B.; Ju, J.; Kobayashi, H.; Kutteh, R.; Lin, Z.; Littlefield, R.; Long, X.; Meng, B.; Nakajima, T.; Niu, S.; Rosing, M.; Sandrone, G.; Stave, M.; Taylor, H.; Thomas, G.; van Lenthe, J.; Wong, A.; Zhang, Z. *NWChem*, a computational chemistry package designed to run on high-performance parallel supercomputers, version 4.5; Pacific Northwest National Laboratory: Richland, WA, 2003.

(86) King, H. F.; Stanton, R. E.; Kim, H.; Wyatt, R. E.; Parr, R. G. *J. Chem. Phys.* **1967**, *47*, 1936−1941.

(87) Pietro, W. J.; Francl, M. M.; Hehre, W. J.; Defrees, D. J.; Pople, J. A.; Binkley, J. S. *J. Am. Chem. Soc.* **1982**, *104*, 5039−5048.
(88) Gordon, M. S.; Binkley, J. S.; Pople, J. A.; Pietro, W. J.; Hehre, W. J. *J. Am. Chem. Soc.* **1982**, *104*, 2797−2803.
(89) Binkley, J. S.; Pople, J. A.; Hehre, W. J. *J. Am. Chem. Soc.* **1980**, *102*, 939−947.
(90) Clark, T.; Chandrasekhar, J.; Spitznagel, G. W.; Schleyer, P. V. *J. Comput. Chem.* **1983**, *4*, 294−301.
(91) Li, J.; Fisher, C. L.; Chen, J. L.; Bashford, D.; Noodleman, L. *Inorg. Chem.* **1996**, *35*, 4694−4702.
(92) Baik, M. H.; Friesner, R. A. *J. Phys. Chem. A* **2002**, *106*, 7407−7412.
(93) Brinck, T.; Larsen, A. G.; Madsen, K. M.; Daasbjerg, K. *J. Phys. Chem. B* **2000**, *104*, 9887−9893.
(94) Winget, P.; Weber, E. J.; Cramer, C. J.; Truhlar, D. G. *Phys. Chem. Chem. Phys.* **2000**, *2*, 1231−1239.
(95) Kebarle, P.; Chowdhury, S. *Chem. Rev.* **1987**, *87*, 513−534.
(96) Chowdhury, S.; Heinis, T.; Grimsrud, E. P.; Kebarle, P. *J. Phys. Chem.* **1986**, *90*, 2747−2752.
(97) Martin, R. L.; Hay, P. J.; Pratt, L. R. *J. Phys. Chem. A* **1998**, *102*, 3565−3573.
(98) Zhan, C. G.; Dixon, D. A. *J. Phys. Chem. A* **2002**, *106*, 9737−9744.
(99) Miertus, S.; Tomasi, J. *Chem. Phys.* **1982**, *65*, 239−245.
(100) Miertus, S.; Scrocco, E.; Tomasi, J. *Chem. Phys.* **1981**, *55*, 117−129.
(101) Barone, V.; Cossi, M.; Tomasi, J. *J. Chem. Phys.* **1997**, *107*, 3210−3221.
(102) Ketkar, S. N.; Kelley, M.; Fink, M.; Ivey, R. C. *J. Mol. Struct.* **1981**, *77*, 127−138.
(103) Slouf, M. *J. Mol. Struct.* **2002**, *611*, 139−146.
(104) Fu, Y. G.; Brock, C. P. *Acta Crystallogr. Sect. B* **1998**, *54*, 308−315.
(105) Karolak-Wojciechowska, J.; Socha, A.; Trzezwinska, H. B. *Pol. J. Chem.* **1996**, *70*, 111−117.
(106) Ball, B.; Zhou, X. F.; Liu, R. F. *Spectrochim. Acta, Part A* **1996**, *52*, 1803−1814.
(107) Martin, J. M. L.; ElYazal, J.; Francois, J. P. *J. Phys. Chem.* **1996**, *100*, 15358−15367.
(108) Siebrand, W. *J. Chem. Phys.* **1964**, *41*, 3574−3581.
(109) Coulson, C. A.; Rushbrooke, G. S. *Proc. Cambridge Philos. Soc.* **1940**, *36*, 193−200.
(110) Wardman, P. *J. Phys. Chem. Ref. Data* **1989**, *18*, 1637−1755.
(111) Chipman, D. M. *J. Phys. Chem. A* **2002**, *106*, 7413−7422.
(112) Larsen, H.; Pedersen, S. U.; Pedersen, J. A.; Lund, H. *J. Electroanal. Chem.* **1992**, *331*, 971−983.
(113) Jakobsen, S.; Mikkelsen, K. V.; Pedersen, S. U. *J. Phys. Chem.* **1996**, *100*, 7411−7417.
(114) Legros, B.; Vandereecken, P.; Soumillion, J. P. *J. Phys. Chem.* **1991**, *95*, 4752−4761.